Green synthesis of positive electrodes for high performance structural batteries - A study on graphene additives

Composites Science and Technology 251 (2024) 110568

Contents lists available at ScienceDirect

Composites Science and Technology

journal homepage: www.elsevier.com/locate/compscitech

Green synthesis of positive electrodes for high performance structural batteries - A study on graphene additives

Zhenyuan Xia [a,b,*,1], Zhaoyang Li [a,1], Johanna Xu [a], Sankar Sasidharan [a], Jaime S. Sanchez [c], Vincenzo Palermo [a,b], Leif E. Asp [a]

[a] Industrial and Materials Science, Chalmers University of Technology, Hörsalsvägen 7B, 41258, Göteborg, Sweden
[b] Istituto per la Sintesi Organica e la Fotoreattività, CNR, via Gobetti 101, 40129, Bologna, Italy
[c] Electrochemical Processes Unit, IMDEA Energy Institute, Móstoles, 28935, Spain

ARTICLE INFO

Handling Editor: Marino Quaresimin

Keywords:
Carbon fibre
Structural batteries
Electrophoretic deposition
Green synthesis
Graphene additives

ABSTRACT

Carbon fibres (CF) have the potential to serve as versatile and multifunctional conductive electrodes within the concept of "structural batteries". These batteries possess the unique ability to both store electrical energy and bear mechanical loads without requiring extra current collectors. However, numerous challenges remain on the path to commercializing structural batteries. One significant challenge lies in the fabrication process of CF-based cathode composites, including the poor adhesion of active materials to the CF surface and the use of hazardous organic solvents, such as *N*-methyl pyrrolidone (NMP) through traditional blade coating. In this study, we present a sustainable fabrication approach, using electrophoretic deposition (EPD) to construct positive electrode composites with lithium iron phosphate ($LiFePO_4$) and graphene nanosheets. Especially, ethanol was used as a green solvent replacing NMP to minimize the environmental impact. Meanwhile, the influence of different types of graphene additives (three kinds of graphene nanoplatelets (GNP), four kinds of reduced graphene oxide (rGO) and one home-made graphene) to the relative battery performance were evaluated under a systematic comparative analysis. Among the tested graphene additives, LFP/rGO2 based positive electrode exhibits a desirable specific capacity of 126.2 $mAhg^{-1}$, maintaining over 93% retention even under the demanding conditions of 2C over 500 cycles.

1. Introduction

The increasing demand for energy and the accompanying environmental impact of CO_2 emission, mainly from fossil fuels, have urged the search for sustainable energy generation/storage solution [1]. There has been a transition in the automotive industry towards electric-powered and lightweight vehicles, that can achieve zero-emission with a reduced carbon footprint.

Differently from the traditional metallic structures (e.g., steel, aluminium) that provide a mechanical load to the vehicles, carbon fiber (CF) based structural battery composites can not only serve as structural components but also provide energy storage capability, thus giving extra energy and power with a significant weight reduction and increased energy efficiency of vehicles [2–5]. These advanced lightweight composite materials with excellent stiffness and strength-to-weight ratio could potentially replace the inert component metal materials currently used in car body panel manufacturing [6]. A typical structural battery composite consists of a laminated battery architecture, in which two different CF layers work as positive and negative electrode tows, and the electrolyte is present within pores of a polymer matrix combining the two layers and a separating glass fiber fabric [6]. Like graphite, CF tows can be directly applied as the negative electrodes in Li-ion batteries. However, as positive electrodes CF tows are electrochemically inactive, they must be functionalized with active materials, for example, lithium-based compounds like iron phosphate (LiFePO4, or LFP), to form positive electrode (or cathode) composite lamina [7,8]. Standard coating techniques like blade coating or spray coating can be used for this functionalization, although the complex geometry of CF tows renders makes it difficult to obtain a uniform coating over the cylindric, entangled surface of the CF tows [9,10]. Moreover, all these processes need to use high-boiling organic solvents such as N-methyl pyrrolidone (NMP) which require a time-consuming long drying process.

* Corresponding author. Industrial and Materials Science, Chalmers University of Technology, Hörsalsvägen 7B, 41258, Göteborg, Sweden.
E-mail address: zhenyuan@chalmers.se (Z. Xia).
[1] Zhenyuan Xia and Zhaoyang Li contributed equally to this manuscript.

https://doi.org/10.1016/j.compscitech.2024.110568
Received 31 March 2023; Received in revised form 5 November 2023; Accepted 22 March 2024
Available online 26 March 2024

We demonstrated in our recent work that electrophoretic deposition (EPD) can be used to effectively coat complex substrates like CF tows, without using NMP solvent (see in Scheme 1) [11]. EPD uses an applied electric field to deposit on a conductive substrate charged particles, suspended in a colloidal dispersion [12,13] and is a cost-effective method in material processing to provide homogeneous and dense layer of functional composite coating on any arbitrary shape, even on 3D irregular shapes like individual CF surface [14]. High-performance electrodes for Li-ion batteries have been reported using the EPD approach, with better performance in comparison to those realized with traditional wet coating methods [15,16]. Recently, Hagberg et al. coated different mixtures of LFP, carbon black (CB) and polyvinylidene fluoride (PVDF) onto T800 CF in acetone solvent [17]. The sample coated with a ratio of 90:6:4 (LFP: CB: PVDF) showed the best performance and delivered a specific capacity of 110 mAh/g with good stability and a capacity retention of ca. 50 % after 1000 cycles. Apart from that, we have previously reported electrochemical techniques to construct positive electrodes with LFP and graphene additives [11]. Further, we also achieved significant improvements in cathode performance by adding nanosheets of electrochemically exfoliated graphene oxide (EGO) during the EPD fabrication process in dimethylformamide (DMF) solvent [18,19]. The studies demonstrated the potential of graphene/LFP based composite cathodes in a full cell, with a pristine CF negative electrode and LFP/EGO coated CF cathode in liquid electrolyte, where a maximum specific capacity of 79.85 mAh/g with 88.1 % capacity retention at 1 C over 300 cycles was achieved. This excellent cycling behaviour could be attributed to the efficient charge transfer from graphene additives, that prevents capacity fade via the favourable mass balance between electrodes and formation of uniform and continuous conductive networks in the bulk of electrodes [10,11,20,21].

Although graphene additives can boost the electrochemical performance of LFP based electrode composites, the toxicity of DMF solvent is forcing us to find greener and more environmentally friendly solvents for the EPD technique. There are many commercially available conductive graphene related materials (GRM), which are generally categorized into two types: reduced graphene oxide (rGO) and graphene nanoplatelet (GNP). To the best of our knowledge, there is no report about the influence of different graphene additives in LFP based Li-ion batteries, not to mention the structural batteries. In the present study, we performed a comparative study on the impact of various graphene additives on the electrochemical performance on positive electrodes of structural battery. The different graphene additives studied include our home-made EGO along with commercially available GNPs (3 types), and rGOs (4 types). Finally, for the EPD process, ethanol was used as the environmentally sustainable solvent, instead of DMF.

2. Experimental

The reagents used for synthesis and experiments were analytical grade and employed as received, without any further purification. Distilled water was used in all the experiments.

2.1. Electrophoretic deposition (EPD) of $LiFePO_4$/graphene

Polyacrylonitrile (PAN) based carbon fibre tow (T800SC-12K-50C, Toray) composed of 12,000 filaments with a linear tow weight of 0.52 g/m was used as the starting material. As-received carbon fibres were cleared with refluxed dichloromethane overnight to remove the polymer sizing agents before deposition. EGO was prepared using an electrochemical exfoliation method reported by the authors previously [19]. rGO and GNP samples were purchased from different companies (see Table S1). $LiFePO_4$/EGO samples were synthesized via EPD involving the following steps: 500 mg carefully grinded $LiFePO_4$ (LFP) particles (MTI Corporation average particle size 3.5 μm) were dispersed in 50 mL of Ethanol using a Sonics VCX-750 Vibra-Cell ultrasonic liquid processor (10 min). This process aimed to create stable $LiFePO_4$ (LFP) dispersions and reducing the particle size. Subsequently, the surface charge of LFP particles in the solution was adjusted by slowly introducing 1 ml of Ethanol (EtOH) containing 500 μL of poly diallyldimethylammonium chloride (PDDA; 20 wt % in H_2O), which had been previously dissolved in a batch sonicator. A 50 mL solution of graphene additive (EGO or rGO or GNP) in EtOH solution (0.50 mg/ml) was combined with carbon black (CB, Super P, ~ 40 nm, 0.50 mg/ml). CB was used as a micro-additive to further enhance the conductivity. The PDDA/LFP dispersion was mixed with graphene/CB dispersion under sonication for another 10 min. The weight distribution of all components in the final suspension was as follows: $LiFePO_4$ at 90 wt %, graphene additive at 5 wt % and CB at 5 wt %. Given that the multi-composite particles carried a positive charge due to the PDDA charging agent, these charged colloids or particles within the suspension migrated towards the cathode side upon the application of an electric field, ultimately forming a coherent deposit on CF electrode surface. The deposition process was accomplished by cathodic electrophoresis in an organic medium, offering the advantage of preventing water electrolysis and mitigating oxidative damage to the active materials on anode surface. The working electrode (WE) was composed of a bundle of CF with 60 mm in length and 15 mm in width. A stainless-steel plate, sized at 80 mm × 20 mm, served as a counter electrode, positioned in parallel to the CFs at a distance of 40 mm. The EPD coating was achieved by applying a direct current (DC) potential of 70 V for a duration of 20 min. Notably, no additional polymer binders were utilized.

2.2. Microstructural characterization

Scanning electron microscopy (SEM) and energy dispersive X-ray spectroscopy (EDX) were used to investigate the quality and composition of the EPD coating deposited onto the CF. SEM images of the samples along with EDX having elemental mapping were collected using a JEOL JSM-7800F Prime at an acceleration voltage of 8 kV. Zeta potential and DLS measurement were conducted by Malvern DLS/Zetasizer

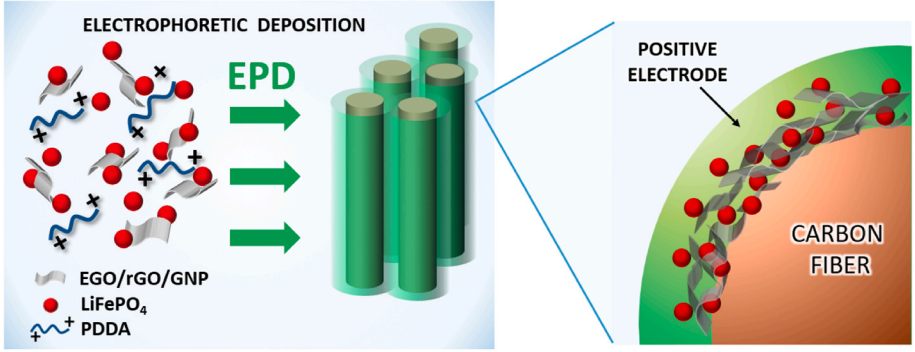

Scheme 1. Schematic illustration about green synthesis of $LiFePO_4$ positive electrodes with graphene additives via EPD approach.

Nano while Raman spectra were recorded using a Raman microscope (alpha300 R, WiTech) with an Nd: YAG laser (532 nm wavelength) and an optical objective of 50X, using an integration time of 0.5 s.

2.3. Half-cell assembly and characterization

The liquid electrolyte was prepared in a glovebox having an Argon atmosphere. A Lithium (Li) foil was used as the anode, while $LiFePO_4$/EGO coated CF acted as the cathode, and glass microfiber filter paper served as the separator. The pouch cell bags were composed of multiple layers of PET/Al/PE, having a total thickness of less than 100 μm. Nickel current collectors were connected to the Li foil, and aluminium current collectors were attached to the positive electrode CFs. Before sealing the pouches, the separator was impregnated with 400 μL of electrolyte made of 0.6 M lithium triflouromethanesulfonate (LiTf) and 0.4 M lithium bis (oxalato)borate (LiBoB) in a 1:1 wt ratio of ethylene carbonate (EC): propylene carbonate (PC). The pouch cells were manufactured inside a glove box under an inert atmosphere with less than 1 ppm O_2 and H_2O at ambient temperature. The finished pouch cell had dimensions of 80 mm × 60 mm. After assembly, half cells were analysed through Galvanostatic Charge/Discharge (GCD) and Electrochemical Impedance Spectroscopy (EIS) measurements, with cycling performance tested over 500 cycles at 2C.

GCD cycles were conducted between 2.6 and 4.2 V vs. Li/Li^+ at various rates using the Bio-Logic BCS-805 station. All charge/discharge cycles were recorded for up to 500 cycles at 1C. EIS measurements were performed in the frequency range from 100 kHz to 0.1 Hz under an alternating current (AC).

Specific capacity of the samples was calculated from discharge curves according to Ref. [11]:

$$Q = \frac{\int I dt}{m} \quad (1)$$

Where Q is the specific capacity ($mAh{\cdot}g^{-1}$) based on the total electrode mass electrodeposited, I is the current, and m is the mass of the electrodeposited material (g) and dt is the time differential.

3. Results and discussion

3.1. Dispersion study of the graphene materials

To evaluate the performance when using different graphene additives in the structural battery cathode (positive electrode) fabrication process, we chose 8 different kinds of graphene additives (Table S1), to prepare the dispersions. These include a home-made electrochemically exfoliated graphene oxide (EGO) along with commercially available GNPs (3 types), and rGOs (4 types). The reason to select these samples is that most of them are representative of graphene-based products from the market, and the materials from each group (rGO and GNP) possess varying specific surface area value (83-745 $m^2\ g^{-1}$), depending on their production and availability on the kilogram scale or even ton scale, as reported in the previous work [22].

A stable dispersion of additives is critical for the successful EPD process and in this work, we choose ethanol (EtOH) as a green solvent for the EPD of positive electrode materials instead of other toxic organic solvents such as NMP and DMF. EtOH is also a volatile solvent (boiling point: 78.3 °C), which facilitates the removal of solvent residue after the EPD step. Initially, the stability behavior of the graphene suspensions (0.2 mg/mL) in ethanol was studied with 3 types of commercial surfactants (5 % v/v polymer/EtOH), including two cationic polymers: polydiallyldimethylammonium chloride (PDDA), polyethylenimine (PEI), and one non-ionic surfactant octyl phenol ethoxylate ether (Triton X-100). Fig. 1 shows that after overnight storage, all graphene samples, except for rGO1, exhibited good dispersion stability in PDDA/EtOH solvent. Meanwhile, none of the samples was stable in PEI/EtOH medium with visible sedimentation, and only rGO3, GNP2 were well dispersed in Triton X-100. This could be attributed to the effective electrostatic stabilization of positively charged graphene in PDDA/EtOH.

A further study on zeta potential (ζ) measurement confirmed that surface charges stabilize graphene dispersions in PDDA/EtOH. ζ values of EGO, rGO2, rGO3, rGO4, GNP1, GNP2 and GNP3 in PDDA were +32.7 ± 1.8 mV, +30 ± 2.0 mV, +25.5 ± 0.9 mV, +26.3 ± 4.4 mV, +12.3 ± 2.6 mV, +23.3 ± 1.7 mV, and +15.7 ± 3.1 mV, respectively (Fig. 2a). The positive values of these samples, in the range of 12–32 mV, indicate the good stability of graphene dispersions assisted by the cationic stabilizer PDDA. A ζ value close to zero (0.3 ± 0.4 mV) observed for rGO1 indicates low surface charge on rGO1 surface, which explains the sedimentation phenomenon of rGO1 in PDDA/EtOH. In comparison, graphene dispersions in PEI/EtOH solution reveal lower positive ζ values than the ones in PDDA/EtOH(see Fig. 2a and Table S2). Meanwhile, in Triton solution, only rGO3 and GNP2 show a reasonable negative zeta potential value of −30.6 mV ± 4.2 and −39.2 ± 3.0 mV. The result validates what was visually observed, as depicted in Fig. 1. These findings can be explained by the differences in the chemical nature of the selected three surfactants: 1) PDDA is a strong cationic polyelectrolyte with highly charged quaternary ammonium groups. In addition, the existence of unsaturated side chains in PDDA facilitates the π-π interaction between the graphene sheets and PDDA backbones. Both strong electrostatic attraction and the π-π interaction promote net positive charges on all graphene surfaces. 2) PEI is a weak linear cationic polyelectrolyte, and the polymer's charge increases with decreasing pH

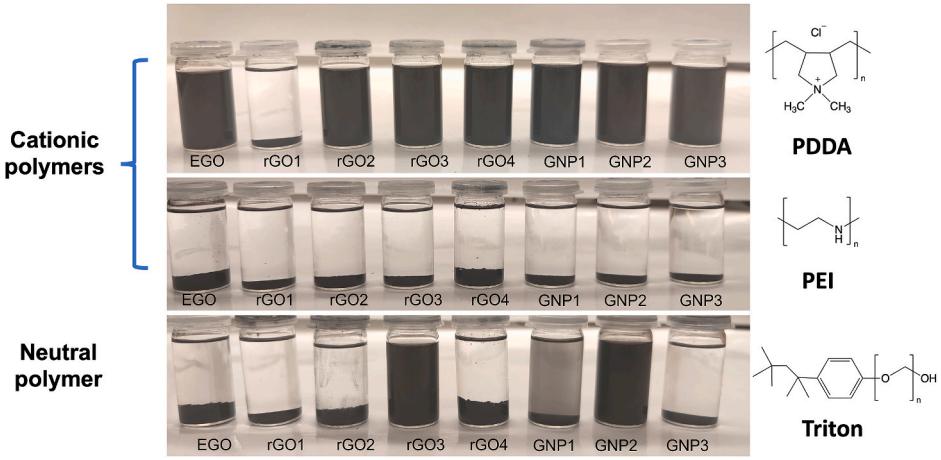

Fig. 1. Photographs of different graphene-based material in ethanol solution with 3 different types of polymer stabilizers after standing overnight.

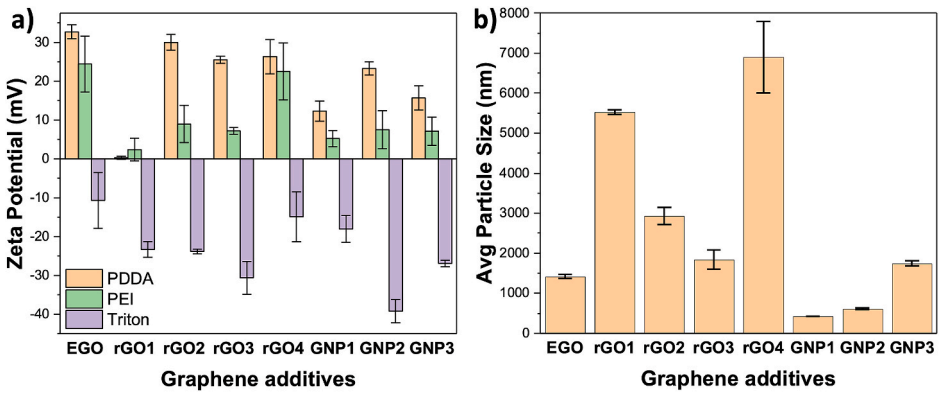

Fig. 2. a) Zeta potential and b) particle size distribution (DLS) data of different graphene dispersion in EtOH solvent with PDDA (5 v.v.%).

values. In EtOH solvent, it behaves like neutral water solution, with few amine groups on PEI being protonated. Thus, there are less positively charged PEI molecules anchored to graphene and there is no π-π interaction between PEI and graphene. 3) Triton is a nonionic surfactant that contains alkyl phenol groups. These aromatic phenol species exhibit a robust π-π interaction with graphene substrate. However, neutral surfactant Triton will not change the negative electric charge of the graphene surface. Although it helps for the dispersion of some graphene samples like rGO3 and GNP2, the negatively charged graphene nanosheets cannot be used for cathodic electrophoretic deposition in our work.

Fig. 2b shows the size distribution of dispersed graphene samples in PDDA/EtOH by dynamic light scattering (DLS). DLS provides the hydrodynamic radius of target particles, which is indicative of the apparent size adopted by graphene samples in EtOH [23]. Average particle size value of all rGO samples were higher than EGO and GNP ones, with the decreasing trend: rGO4 (6895 ± 890 nm) > rGO1 (5526 ± 50 nm) > rGO2 (2933 ± 211 nm) > rGO3 (1843 ± 245 nm) > GNP3 (1743 ± 65 nm) > EGO (1421 ± 54 nm) > GNP2 (612 ± 24 nm) > GNP1 (422 ± 3.2 nm).

3.2. Morphology and structure study of the graphene materials

To further define the particle size and surface morphology of different graphene materials, SEM images of these samples dispersed in EtOH and then spin-coated on silicon wafer were recorded as shown in Fig. 3. Compared to rGO samples, GNPs showed a lamellar structure with thicker layers, while large flakes with thinner and crumpled morphology were observed in the rGO materials. These crumpled or folded flakes are due to the intersheet interactions among the oxygen functional groups on rGO surface [22,24]. Graphene flakes with the lateral size over tens of microns could be easily found for the rGO4 sample, and the rest of the rGO samples showed similar lateral size and surface morphology. In the case of EGO, the flake structures were similar to rGO samples, but showed better adhesion to the silicon wafer substrate, in which sheet-like morphology with overlapped EGO flakes can be easily observed (see Fig. 3a). It is worth mentioning that the morphology of GNP1 was totally different from other graphene samples where clusters of nanoparticles with spherical architectures were observed (see inset of Fig. 3b).

Fig. 4 displays the Raman spectra of all graphene samples. Among them, two characteristic peaks at around 1346 cm^{-1} (D band) and around 1572–1596 cm^{-1} (G band) can be easily identified. The D band is produced by out-of-plane vibrations due to structural defects while the G band originates from the in-plane vibrations of sp^2 carbons [18]. The value of G band for GNP2 and GNP3 were at 1572 cm^{-1} and 1578 cm^{-1}, respectively, which is consistent with the value of pristine graphene G band. For all other samples, the G band has broadened and shifted to higher wavelengths (rGO1: 1581 cm^{-1}; rGO2: 1583 cm^{-1}; rGO3: 1590 cm−1; rGO4: 1587 cm^{-1}, GNP1: 1593 cm^{-1}, EGO: 1596 cm^{-1}) due to

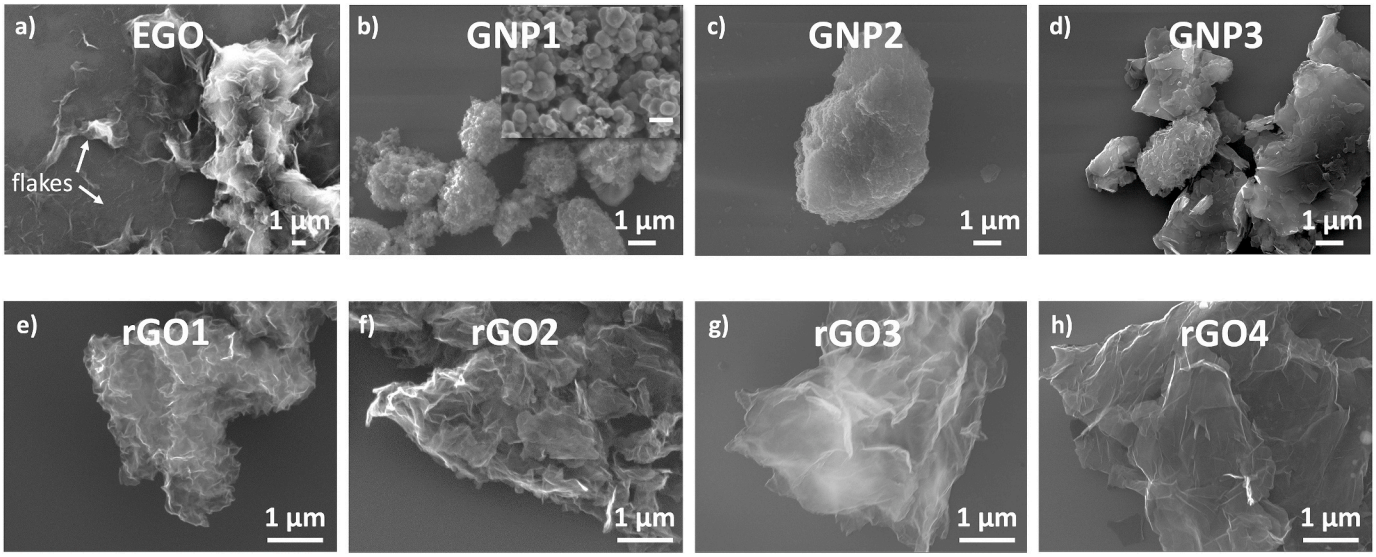

Fig. 3. SEM images of different kinds of starting graphene materials: a) EGO, b) GNP1, c) GNP2, d) GNP3, e) rGO1, f) rGO2, g) rGO3, h) rGO4. (*The inset of 3b) shows the high-resolution image of GNP1 flakes with scale bar* 100 *nm*).

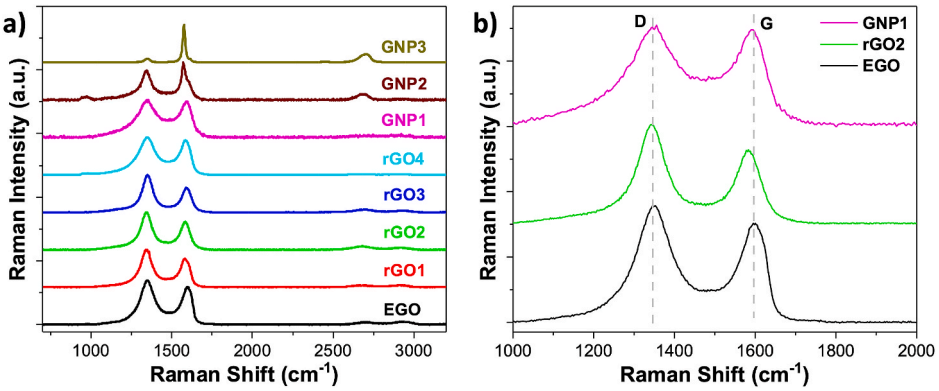

Fig. 4. a) Raman spectra of different types of graphene materials used in the study, b) zoom-in area of EGO, rGO2 and GNP1 materials within the D and G peak range.

the oxidation induced defects. The defect level can be evaluated by the intensity ratio of D band and G band [18], and the (I_D/I_G) ratio increases with the trend: GNP3 (0.19) < GNP2 (1.28) < GNP1 (1.47) < EGO (1.49) < rGO4 (1.53) < rGO2 (1.64) < rGO1 (1.69) < rGO3 (1.77). The high I_D/I_G value from all rGO samples and EGO is due to the small sp^2 domains and distortions created by either the reduction of graphene oxide or the electrochemical process. It is interesting that GNP1 also has a high I_D/I_G value (1.28), with a broadener D and G band, as compared to the bands of rGO and EGO (see Fig. 4). The high defect level of GNP1 might come from the pyrolysis process of waste tires during their synthesis. 2D band is the secondary D band at around 2700 cm^{-1}, which is usually used for determining the number of graphene layers and in our case, all of the rGO, EGO and GNP1 samples showed a broad and low intensity 2D band. This is possibly attributed to oxidation during the fabrication process that broke the stacking order of adjacent graphene layers and introduced amorphization of carbon atoms [18,25]. The features in the Raman spectrum clearly corroborate the phenomena observed in the SEM.

3.3. Structural study of the electro-deposited LFP/graphene composites

The electrophoretic deposition process for the fabrication of LFP/graphene composites on carbon fibers was the same as our previous report [11]. In the present work, EtOH was used as the solvent instead of DMF for all EPD experiments. It is worth nothing that the dielectric constant of the two solvents is different (ε_{DMF}: 36.7, ε_{EtOH}: 24.5). A solvent with a higher dielectric constant will intensify the polarization effect on the LFP target particles, thereby enhancing the ability of the negative electrodes to attract the nanocomposites out of the solution. On the other hand, ethanol, with its lower dielectric constant, is not as effective as DMF in the EPD process. Hence, we opted for a deposition time of 20 min. PDDA, a long-chain cationic polymer featuring positively charged quaternary ammonium ring groups along with free chloride, was chosen to serve the dual role of providing surface charge and acting as a stabilizer to prevent aggregation of graphene flakes in our multi-component suspension (Scheme 1). Positive charges introduced from the quaternary cations will facilitate the deposition of LFP/graphene particles to the negative electrodes, while the long alkyl chains from PDDA helps in suppressing the aggregation and maintain the stability of the suspension during the coating [11]. After EPD, the microstructure of fabricated composites was studied by SEM microscopy (see Fig. 5 and Fig. S1). A control sample without graphene additives was also made to understand the effect of graphene in all composite electrode materials. All coated samples with graphene showed similar morphology, with the LFP/graphene coating covering almost the whole CF surface. LFP particles with sub-micrometer size were well dispersed on the fiber surface, wrapped, or partially covered by different graphene flakes. All GNP samples with flat and thick nanosheets incorporated with LFP particles were visible in the relative SEM images. In the case of rGO and EGO samples, especially for rGO1, highly wrinkled layers with

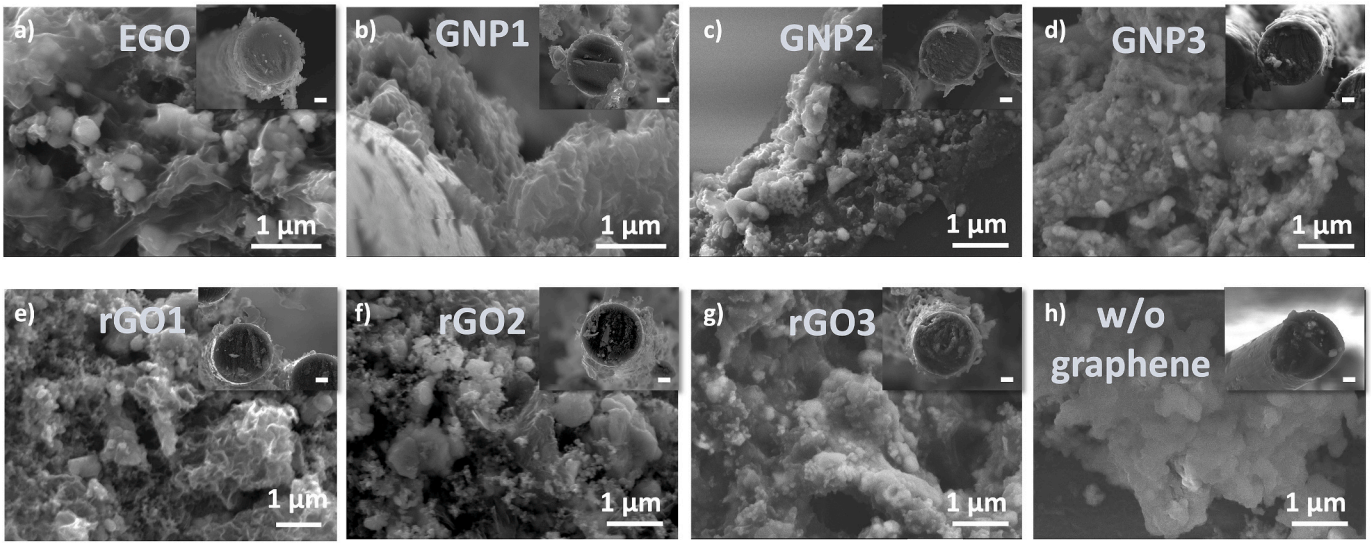

Fig. 5. SEM images of LFP and different graphene additives coated on CF substrates, a) LFP/EGO, b) LFP/GNP1, c) LFP/GNP2, d) LFP/GNP3, e) LFP/rGO1, f) LFP/rGO2, g) LFP/rGO3, h) LFP without graphene (*the insets show the coating from a cross section with scale bar* 1 μm).

irregular shapes of graphene flakes were observed on CF matrix. Compared with rGO and GNP samples, EGO additive shows a smoother surface with consistent distribution of LFP particles wrapped on the fiber surface. As for the control sample, only the aggregated LFP particles unevenly distributed on CF surface were observed.

A comparison of the Raman spectra of the EGO, rGO and GNP composites further confirmed successful combination of LFP particles and graphene layers (Fig. S2). The Raman spectra of all LFP/graphene composites show intense peaks ascribed to the orthorhombic $LiFePO_4$ phase, including the vibrations modes of PO_4^{3-} tracked at 431, 581, 988 and 1031 cm^{-1} and the vibrations modes attributed to Fe-O at 214, 277, 449 cm^{-1} [11,26]. While the D and G band from graphene were overlapped with the CF substrate (D band: 1351 cm^{-1}, G band: 1581 cm^{-1}), which makes it difficult to identify the contribution from graphene additives.

3.4. Electrochemical characterization of the coated CF electrodes

The influence of different graphene additives on the electrochemical behaviour for structural battery composites were studied in half-cell devices. Fig. 6a–S3a, and S4a shows the CV curves of the samples coated at different deposition times with a scan rate of 0.1 $mV \cdot s^{-1}$ in the 2.6V-4.2V vs Li^+/Li voltage range. Positive electrodes based on rGO2 and GNP1 were selected from the two types of graphene starting materials, to compare with the EGO sample and LFP coating without graphene additive was used as the control. The three devices with graphene additives displayed typical oxidation/reduction peaks during the anodic/cathodic scan arising from the reversible faradaic redox reaction Fe^{2+}/Fe^{3+} in $LiFePO_4$ particles, which agrees with previous reports [11,27,28]. All devices presented sharp and symmetric peaks with a small potential difference between the anodic and cathodic peaks (EGO: 0.31 V; rGO2: 0.36 V; GNP: 0.32 V), indicating low polarization and high redox reversibility of the composites. Instead, the control sample without graphene additives showed a wider and less intense peak with potential intervals between the peaks of 0.43 V, demonstrating the beneficial role of graphene additives in improving the conductivity of positive electrodes and enhancing the electron transfer during oxidation and reduction process [11,26,29,30]. However, an irreversible oxidation peak at around 4.0 V was observed for all graphene-based electrodes during the first few CV cycles (Fig. 6a, S3a, and S4a), possibly due to the remaining oxygen functional groups or impurities from the starting graphene materials.

Fig. 6b and Figs. S3b and S4b displays the first charging and discharging profiles of the four samples prepared with or without graphene additives, measured at low (0.1C) or high (2C) charging rates. At 0.1C, all LFP samples with graphene additives showed comparable performance, much better than the control sample. At high charge/discharge rate (2C), the composite LFP/EGO showed the highest specific capacity of all samples. The control sample without graphene additives showed a rather low-capacity value at 2C, due to the poor charge transfer interaction between the active LFP material and the CF substrates. The average plateau at around 3.5 V vs Li^+/Li during charge and at around 3.4 V vs Li^+/Li during discharge also indicates a typical battery type performance with Fe^{2+}/Fe^{3+} redox reaction [11,31], and the results fit well with the observed redox peaks in CV curves. The polarization between the charging and discharging plateaus for the LFP/EGO, LFP/rGO2, LFP/GNP1, and control samples were 0.06 V, 0.08 V, 0.05 V, and 0.10 V respectively. Again, the lower polarization of the graphene-based devices is attributed to the low internal resistance, in agreement with the cyclic voltammograms (Fig. 6a). Similar electrochemical performance was detected in all other rGO and GNP related half-cell devices.

Fig. 6c, **S3c, and S4c** compare the rate capability of positive electrodes with graphene additives at different C-rates (0.1C, 0.2C, 0.5C, 1C and 2C). The LFP/rGO2 composite exhibited the best capacity value at low-rate, delivering a discharge capacity of 126.2 mAh g^{-1} at 0.1 C. On the other hand, the LFP/EGO composite revealed the best high-rate performance with a discharge capacity value of 61.7 mAh g^{-1} at 2 C and a good capacity retention of 58.2 % from 0.1 C (106.1 mAh g^{-1}). The other three rGO-based composites also demonstrated similar low-

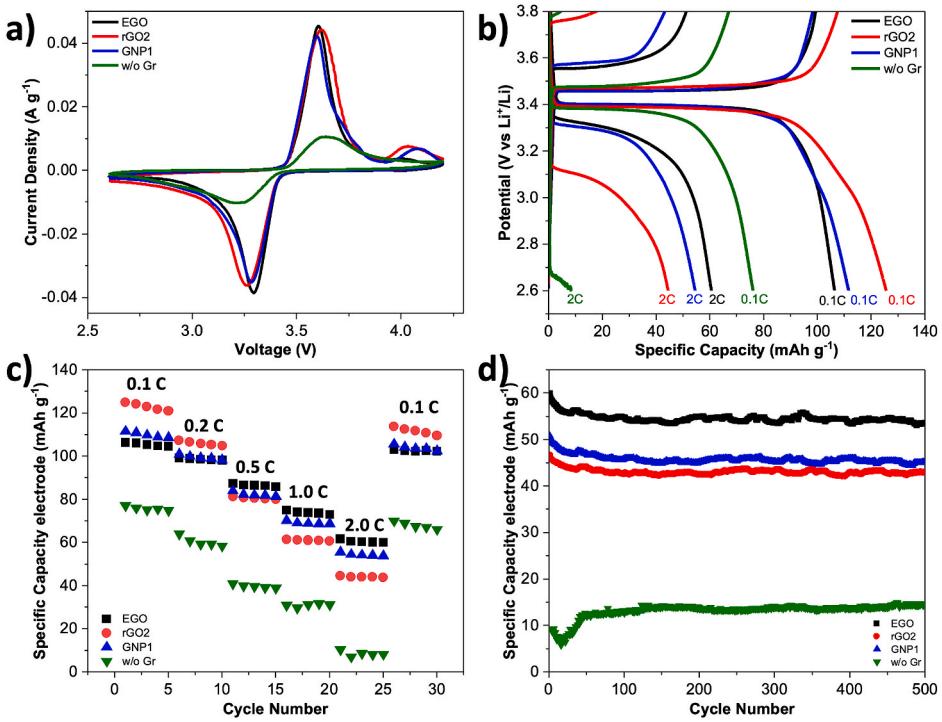

Fig. 6. Electrochemical evaluation of the LFP with different kinds of graphene additives as positive electrode materials: (a) CV of the LFP/EGO, LFP/rGO2, LFP/GNP1, and without graphene additives at a scan rate of 0.1 mV s^{-1} in 2.6–4.2 V vs. Li^+/Li. (b) Comparison of the first charging and discharging profiles of the four samples at a low (0.1C) and high rates (2C). (c) Specific capacities of the four samples at various C-rates. (d) Cycling stability of the four samples cycled at 2C.

rate capacity as LFP/rGO2, with the highest value of 100.8 mAh g^{-1} for LFP/rGO1, 101.1 mAh g^{-1} for LFP/rGO4, and even 140.9 mAh g^{-1} for LFP/rGO3 at 0.1 C. However, the high-rate performance of the three rGO samples was worse than using EGO with LFP/rGO2 holding a capacity value of 44.5 mAh g^{-1}, while LFP/rGO1 and LFP/rGO3 showing values of 34.8, and 44.0 mAh g^{-1} respectively. In addition, the LFP/rGO4 composite proved to be unstable during the high-rate charge/discharge process, resulting in device failure at 0.5 C rate. While testing the GNP samples, LFP/GNP1 showed similar electrochemical performance to the LFP/EGO device, with a discharge capacity of 110.2 mAh g^{-1} at 0.1 C and 57.0 mAh g^{-1} at 2 C, comparable to EGO and rGO2. Other two GNP based devices demonstrated worse discharging capacities, especially at high-rate: 131.8 mAh g^{-1} at 0.1 C and 32.1 mAh g^{-1} at 2 C for LFP/GNP2, and 86.9 mAh g^{-1} at 0.1 C and 24.4 mAh g^{-1} at 2 C for LFP/GNP3. In comparison to all the above results, the control device without any graphene additives displayed the lowest electrochemical performance, with a discharge capacity of 77.2 mAh g^{-1} at 0.1 C and 10.5 mAh g^{-1} at 2 C.

The rate capacity performance of these samples is reproducible and stable, as proved by the restoration of initial capacity after returning to 0.1 C. This behaviour clearly indicates good adhesion of graphene flakes with the active materials during the charge/discharge process. Further, SEM analysis of the samples after cycling confirmed that there was no detachment of active LFP particles or debonding of the graphene additives on CF matrix (see Figs. S5 and S6), except rGO4 based sample. A spotless and smooth surface of the CF without any discernible representation of LFP particles or rGO flakes reveals the reason for detachment in LFP/rGO4 during the cycling process, further explaining the failure of rGO4 based half-cell. The failure of rGO4 is confirmed by conducting repeated experiments. This phenomenon can be attributed to the significant size difference between the large rGO4 flakes (up to 240 μm [22]) and the small dimensions of the carbon fiber matrix (with an average diameter of 5–10 μm), the nearly 50-fold difference in size between the graphene sheets and the carbon fiber matrix leading to inadequate adhesion and subsequent delamination of the rGO and LFP composites from the fiber surface.

To better understand the electrochemical behaviour of these composites on the positive electrodes, electrochemical impedance spectroscopy (EIS) measurements (Fig. S7 and Table S3) were carried out for all half-cell devices after assembling. The Nyquist plots in EIS demonstrated that the overall impedance of graphene-based samples was much smaller than the control sample without graphene. The intercept on the real axis in the high-frequency region (R_s) of the EIS spectra was comparable for all samples (ca. 2-5 Ω cm^{-2}). This value was mostly attributed to the resistance from the electrolyte and electrode. The semicircle observed at high-to-medium frequencies represented the charge transfer resistance (R_{ct}) on the electrode. Notably, most of the graphene samples showed a R_{ct} value of around 20 Ω. Without graphene additives, the sample exhibited a significantly higher R_{ct} value of 61.5 Ω. This high value suggests a higher diffusional resistance and poorer surface area for charge transfer compared to most of the samples with graphene additives. In case of rGO4 sample, a relatively high value of 351.2 Ω was obtained, probably due to the large lateral size (from tens to hundreds of micrometres [22]) from rGO4 flakes that hindered ion flow and charge transfer within the positive electrode surface, confirming the battery failure results in Fig. S3c.

Prolonged charge/discharge tests (see Fig. 6d–S3d, and S4d) showed that most of the graphene-based samples have good capacity retention (>80%) after 500 cycles at 2C. Among them, LFP/EGO held the best high-rate capacity of 53.6 mAh g^{-1} with a capacity retention of 90% and discharge capacity of 90.5% at the end of the cycles. All GNP based samples and rGO2 exhibited similar longevity data with high-capacity retention (89.8% for LFP/GNP1; 89.3% for LFP/GNP2; 91.2% for LFP/GNP3; 93% for LFP/rGO2).

The contribution of two important physical and chemical properties, graphene flake size and oxygen content, were summarized with respect to the relative performance of LFP devices at both low and high scan rates, as shown in Fig. S8. Drawing a definitive conclusion on whether EGO, rGO or GNP is better than the other can be challenging. However, for low scan rate, graphene samples with lower oxygen content in either rGO or GNP group exhibited the better electrochemical performance (rGO3: 2.8% oxygen, 140.9 mAh g^{-1} at 0.1 C; GNP2: 6.3% oxygen, 131.8 mAh g^{-1} at 0.1 C). The presence of low oxygen content on graphene might enhance the conductivity of the LFP cathode material, which result in relatively good battery performance. Meanwhile, less oxygen content on graphene surface means less oxygen-functional groups (i.e., hydroxyl, carbonyl, and carboxyl groups) to alter its wettability in EPD process and poor interaction with polar LFP particles. Noteworthy, for high scan rate, rGO3 and GNP2 didn't show the best electrochemical performance. On the contrary, graphene samples with highest oxygen content exhibited best specific capacity at high rate (EGO: 20.4 % oxygen, 61.7 mAh g^{-1}). The high density of oxygen-induced defects did not seem to affect the battery lifetime. In fact, the oxygen-functional groups aid in the dispersion of EGO in ethanol for EPD deposition and enable the better adhesion of LFP particles on CF substrates, which results in the best cycling performance in our work. Besides the intrinsic chemical properties, graphene flake size also affects the final battery performance. The average flake size of rGO group samples was higher than GNP group and EGO samples, which is primarily due to the different fabrication approach used for these materials, as we reported in our previous study [18]. Graphene samples with flake size over 3000 nm (rGO4 and rGO1) showed low-capacity behavior at both low and high rates, especially for rGO4, as we discussed before. All the other samples, except for GNP3, demonstrated reasonable capacity performance at both low and high rate with the average flake size ranging from 422 to 2933 nm. The poor device performance from GNP3 might be due to the hydrophobic nature of pristine GNP3 samples with less defects (lowest I_D/I_G ratio in Fig. 4) and thick layers (see Fig. 3d), which do not readily wet or incorporate with LFP active materials during EPD coating and lead to the poor interaction between CF substrates and active materials. Besides, there is no clear connection between specific surface area of graphene samples and the relative device performance, as we summarized in Table S1, S3 and S8. It is worth noting that there is still room for improvement in optimizing our EPD deposition process with ethanol media, for example, by varying applied potential or deposition time according to different samples. However, even without any optimization, the EPD process has already shown promising results in fabricating LFP/graphene electrodes with comparable specific capacity to that of previously reported EPD coated materials. Besides EGO sample, rGO2 in rGO group samples and GNP1 in GNP group samples with moderate oxygen amount (13.5% for rGO2 and 9% for GNP1) presented robust electrochemical performance at different scan rates. The future work will focus on specific graphene samples like rGO2 and GNP1, to improve their loading capacity and enhance their high-rate performance, in comparison to EGO.

4. Conclusions

In summary, we designed and conducted a study on the dispersion behavior of various types of graphene related materials in ethanol solvent with polymer stabilizers and explored the potential in the development of high-performance positive electrodes for structural batteries. Some commercial rGO and GNP materials exhibited excellent electrochemical performance as additives in structural battery composites. Specifically, the LFP/rGO2 based device showed the highest specific capacity of 126.2 $mAhg^{-1}$ and over 93% retention at 2C over 500 cycles. Our study provides a simple and eco-friendly fabrication process for developing functional coating of graphene-related materials in battery technology. This research presents a promising green deposition process for making functional coating of electrode materials and sheds light on the potential of graphene-related 2D materials in the development of high-performance structural batteries.

Author statement

Zhenyuan Xia Investigation; Writing - Original Draft; Funding acquisition, Zhaoyang Li Methodology Investigation; Writing - Original Draft, Johanna Xu Methodology Investigation; Writing - Review & Editing, Sankar Sasidharan Writing - Review & Editing, Jaime S. Sanchez Writing - Review & Editing, Vincenzo Palermo Conceptualization; Writing - Original Draft, Leif E. Asp Writing - Review & Editing; Funding acquisition.

Declaration of competing interest

The authors declare that they have no known competing financial interests or personal relationships that could have appeared to influence the work reported in this paper.

Data availability

No data was used for the research described in the article.

Acknowledgment

The authors would like to acknowledge Oxeon AB for supplying spread tow carbon fibres. The authors would like to thank the following sources for funding this research: The European Union's Horizon 2020 research and innovation programme under GrapheneCore3 881603 – Graphene Flagship, the Swedish Åforsk Fundation, project no. 222-263; the Swedish National Space Agency, project no. 2020-00256; the strategic innovation program SIP LIGHTer (funding provided by VINNOVA, the Swedish Energy Agency and Formas); Swedish Energy Agency (Project nr 46598-1); 2D TECH VINNOVA competence Center (Ref. 2019-00068); USAF, EOARD Award No. FA8655-21-1-7038; ONR, USA, Award No. N62909-22-1-2037.

Appendix A. Supplementary data

Supplementary data to this article can be found online at https://doi.org/10.1016/j.compscitech.2024.110568.

References

[1] M.M. Titirici, Sustainable batteries-quo Vadis? Adv. Energy Mater. 11 (10) (2021) 2003700.
[2] M.H. Kjell, T.G. Zavalis, M. Behm, G. Lindbergh, Electrochemical characterization of lithium intercalation processes of PAN-based carbon fibers in a Microelectrode System, J. Electrochem. Soc. 160 (9) (2013) A1473–A1481.
[3] R. Pejman, J. Gorman, A.R. Najafi, Multi-physics design of a new battery packaging for electric vehicles utilizing multifunctional composites, Compos. B Eng. 237 (2022).
[4] H. Kuhnelt, A. Beutl, F. Mastropierro, F. Laurin, S. Willrodt, A. Bismarck, M. Guida, F. Romano, Structural batteries for aeronautic applications-state of the art, research Gaps and Technology development needs, Aerospace 9 (1) (2022).
[5] J. Zhang, J. Yan, Y. Zhao, Q. Zhou, Y. Ma, Y. Zi, A. Zhou, S. Lin, L. Liao, X. Hu, H. Bai, High-strength and machinable load-bearing integrated electrochemical capacitors based on polymeric solid electrolyte, Nat. Commun. 14 (1) (2023) 64.
[6] D. Carlstedt, L.E. Asp, Performance analysis framework for structural battery composites in electric vehicles, Compos. B Eng. 186 (2020).
[7] L.X. Yuan, Z.H. Wang, W.X. Zhang, X.L. Hu, J.T. Chen, Y.H. Huang, J. B. Goodenough, Development and challenges of LiFePO4 cathode material for lithium-ion batteries, Energy Environ. Sci. 4 (2) (2011) 269–284.
[8] W.J. Zhang, Structure and performance of LiFePO4 cathode materials: a review, J. Power Sources 196 (6) (2011) 2962–2970.
[9] A. Goren, C.M. Costa, M.M. Silva, S. Lanceros-Mendez, State of the art and open questions on cathode preparation based on carbon coated lithium iron phosphate, Compos. B Eng. 83 (2015) 333–345.
[10] J.W. Jeon, M.C. Biswas, C.L. Patton, E.K. Wujcik, Water-processable, sprayable LiFePO4/graphene hybrid cathodes for high-power lithium ion batteries, J. Ind. Eng. Chem. 84 (2020) 72–81.
[11] J.S. Sanchez, J. Xu, Z.Y. Xia, J.H. Sun, L.E. Asp, V. Palermo, Electrophoretic coating of LiFePO4/Graphene oxide on carbon fibers as cathode electrodes for structural lithium ion batteries, Compos. Sci. Technol. 208 (2021).
[12] O. Hubert, N. Todorovic, A. Bismarck, Towards separator-free structural composite supercapacitors, Compos. Sci. Technol. 217 (2022).
[13] L.H. Ye, K.C. Wen, Z.X. Zhang, F. Yang, Y.C. Liang, W.Q. Lv, Y.K. Lin, J.M. Gu, J. H. Dickerson, W.D. He, Highly efficient materials assembly via electrophoretic deposition for electrochemical energy conversion and storage devices, Adv. Energy Mater. 6 (7) (2016).
[14] L. Besra, M. Liu, A review on fundamentals and applications of electrophoretic deposition (EPD), Prog. Mater. Sci. 52 (1) (2007) 1–61.
[15] X. Michaud, K. Shi, I. Zhitomirsky, Electrophoretic deposition of LiFePO4 for Li-ion batteries, Mater. Lett. 241 (2019) 10–13.
[16] A. Hajizadeh, T. Shahalizade, R. Riahifar, M.S. Yaghmaee, B. Raissi, S. Gholam, A. Aghaei, S. Rahimisheikh, A.S. Ghazvini, Electrophoretic deposition as a fabrication method for Li-ion battery electrodes and separators - a review, J. Power Sources 535 (2022).
[17] J. Hagberg, H.A. Maples, K.S.P. Alvim, J. Xu, W. Johannisson, A. Bismarck, D. Zenkert, G. Lindbergh, Lithium iron phosphate coated carbon fiber electrodes for structural lithium ion batteries, Compos. Sci. Technol. 162 (2018) 235–243.
[18] Z.Y. Xia, S. Pezzini, E. Treossi, G. Giambastiani, F. Corticelli, V. Morandi, A. Zanelli, V. Bellani, V. Palermo, The exfoliation of graphene in liquids by electrochemical, chemical, and sonication-assisted techniques: a Nanoscale study, Adv. Funct. Mater. 23 (37) (2013) 4684–4693.
[19] Z.Y. Xia, G. Giambastiani, C. Christodoulou, M.V. Nardi, N. Koch, E. Treossi, V. Bellani, S. Pezzini, F. Corticelli, V. Morandi, A. Zanelli, V. Palermo, Synergic exfoliation of graphene with organic molecules and inorganic ions for the electrochemical production of flexible electrodes, Chempluschem 79 (3) (2014) 439–446.
[20] J.M. Lu, X.H. Tian, Y.K. Zhou, Y.B. Zhu, Z.H. Tang, B. Ma, G. Wu, T.T. Jiang, X. F. Tu, G.Z. Chen, A novel "holey-LFP/graphene/holey-LFP" sandwich nanostructure with significantly improved rate capability for lithium storage, Electrochim. Acta 320 (2019) 134566.
[21] Y.B. Guan, J.R. Shen, X.F. Wei, Q.Z. Zhu, X.H. Zheng, S.Q. Zhou, B. Xu, LiFePO4/activated carbon/graphene composite with capacitive-battery characteristics for superior high-rate lithium-ion storage, Electrochim. Acta 294 (2019) 148–155.
[22] A. Kovtun, E. Treossi, N. Mirotta, A. Scida, A. Liscio, M. Christian, F. Valorosi, A. Boschi, R.J. Young, C. Galiotis, I.A. Kinloch, V. Morandi, V. Palermo, Benchmarking of graphene-based materials: real commercial products versus ideal graphene, 2D Mater. 6 (2) (2019).
[23] T. Misono, Dynamic light scattering (DLS), in: M. Abe (Ed.), Measurement Techniques and Practices of Colloid and Interface Phenomena, Springer, 2019, pp. 65–69.
[24] R.L.D. Whitby, V.M. Gun'ko, A. Korobeinyk, R. Busquets, A.B. Cundy, K. Laszlo, J. Skubiszewska-Zieba, R. Leboda, E. Tombacz, I.Y. Toth, K. Kovacs, S. V. Mikhalovsky, Driving Forces of conformational changes in single-layer graphene oxide, ACS Nano 6 (5) (2012) 3967–3973.
[25] Z.Y. Xia, G. Maccaferri, C. Zanardi, M. Christian, L. Ortolani, V. Morandi, V. Bellani, A. Kovtun, S. Dell'Elce, A. Candini, A. Liscio, V. Palermo, Dispersion stability and surface morphology study of electrochemically exfoliated bilayer graphene oxide, J. Phys. Chem. C 123 (24) (2019) 15122–15130.
[26] Y. Shi, S.L. Chou, J.Z. Wang, D. Wexler, H.J. Li, H.K. Liu, Y.P. Wu, Graphene wrapped LiFePO4/C composites as cathode materials for Li-ion batteries with enhanced rate capability, J. Mater. Chem. 22 (32) (2012) 16465–16470.
[27] Y. Huang, H. Liu, Y.C. Lu, Y.L. Hou, Q. Li, Electrophoretic lithium iron phosphate/reduced graphene oxide composite for lithium ion battery cathode application, J. Power Sources 284 (2015) 236–244.
[28] C. Chen, G.B. Liu, Y. Wang, J.L. Li, H. Liu, Preparation and electrochemical properties of LiFePO4/C nanocomposite using FePO4 center dot 2H(2)O nanoparticles by introduction of Fe-3(PO4)(2)center dot 8H(2)O at low cost, Electrochim. Acta 113 (2013) 464–469.
[29] Z.Y. Xia, V. Mishukova, S.S. Delekta, J.H. Sun, J.S. Sanchez, J.T. Li, V. Palermo, Selective deposition of metal oxide nanoflakes on graphene electrodes to obtain high-performance asymmetric micro-supercapacitors, Nanoscale 13 (5) (2021) 3285–3294.
[30] J.S. Sanchez, Z.Y. Xia, N. Patil, R. Grieco, J.H. Sun, U. Klement, R. Qiu, M. Christian, F. Liscio, V. Morandi, R. Marcilla, V. Palermo, All-electrochemical nanofabrication of stacked ternary metal sulfide/graphene electrodes for high-performance alkaline batteries, Small 18 (16) (2022).
[31] Z.Y. Xia, M. Christian, C. Arbizzani, V. Morandi, M. Gazzano, V. Quintano, A. Kovtun, V. Palermo, A robust, modular approach to produce graphene-MOx multilayer foams as electrodes for Li-ion batteries, Nanoscale 11 (12) (2019) 5265–5273.